Stagnation point heat flux characterization under numerical error and boundary conditions uncertainty

Michele Capriati, Andrea Cortesi, Thierry E. Magin, Pietro Marco Congedo

Stagnation point heat flux characterization under numerical error and boundary conditions uncertainty

Michele Capriati[a,b,*], Andrea Cortesi[a], Thierry E. Magin[b], Pietro M. Congedo[a]

[a] *Inria, Centre de Mathématiques Appliquées, Ecole Polytechnique, IPP, Route de Saclay, 91120 Palaiseau, France*
[b] *von Karman Institute for Fluid Dynamics, Chaussée de Waterloo 72, 1640 Rhode-Saint-Genèse, Belgium*

Abstract

The numerical simulation of hypersonic atmospheric entry flows is a challenging problem. Prediction of quantities of interest, such as surface heat flux and pressure, is strongly influenced by the mesh quality using conventional second-order spatial accuracy schemes while depending on boundary conditions, which may generally suffer from uncertainty. This paper illustrates one of the first systematic quantification of the numerical error and the uncertainty-induced variability for the simulation of hypersonic flows. Specifically, a mesh-convergence study using grid adaptation tools is coupled with surrogate-based approaches to Uncertainty Quantification. The illustrative example is the simulation of the EXPERT vehicle of the European Space Agency employing the US3D solver.

First, we show the benefits in using mesh adaptation to simulate hypersonic flows under uncertainty. On the one hand, this practice reduces the numerical uncertainty associated with each prediction and, on the other hand, allows us to obtain a more reliable surrogate model for Uncertainty Quantification by preventing non-physical heat flux values.

Secondly, we perform a sensitivity analysis to compare the numerical uncertainty associated with a given mesh with the UQ-induced variability for a specific quantity of interest. In the case considered, the impact of the numerical uncertainty

*Corresponding author. Tel.: +39 340 96 53 013
Email address: michele.capriati@vki.ac.be (Michele Capriati)

turned out to be at least one order of magnitude less than the quantity of interest variability. This result indicates the possibility of using coarse and adapted meshes for future UQ studies.
Keywords: atmospheric entry flows, uncertainty quantification, surrogate model, numerical error.

---

1. Introduction

The numerical simulation of hypersonic flows is a challenging problem, for example in atmospheric entry applications [1, 2], especially when the goal is to obtain reliable and accurate predictions of the thermal loads at the entry vehicle's forebody. In this context, practitioners and experts know the importance of using an appropriate computational grid and mesh adaptation strategy to achieve accurate results. For conventional second-order spatial accuracy numerical schemes, several authors [3, 4, 5, 6, 7, 8, 9, 10] pointed out that:

- A grid-independent solution for the pressure estimation may be inadequate for the heat flux computation.
- A sonic Reynolds number at the wall should be kept under the unity to capture the thermal boundary layer and accurately compute the heat flux.
- Heat transfer prediction is not too much affected by how well the shock is resolved, but the grid must be aligned with the shock shape.
- High cell aspect ratio in the shock region improves the estimation of the heat flux (cells stretched in the shock direction) by preventing the carbuncle phenomenon.
- The choice of grid depends on the numerical scheme used: high-dissipation schemes require higher grid density in the boundary layer, while low-dissipation schemes need a higher quality (grid alignment) in the shock region.

- Hydrodynamic and thermal layers are better resolved when the grid is orthogonal to the surface.

A high-quality computational grid is often the result of some adaptation and monitoring by an expert user [6, 11]. This strategy is normally used to produce a limited number of simulations for well-defined boundary conditions and some prescribed accuracy on a quantity of interest.

It is also important to note that reaching the steady state solution does not necessarily imply a correct result. This may also be affected by uncertainties in the boundary condition and model parameter inputs, or the model choice itself, as well as numerical errors. Uncertainties are related to the governing equations describing for instance high-temperature effects (thermo-chemical non-equilibrium state, dissipative effects such as mass and energy transport, radiation), turbulence, gas-surface interactions (ablation,catalysis), etc. The numerical error is instead related to the computational method and its associated numerical grid used to discretize the physical domain. Both the uncertainties and the numerical error are coupled [12]: for example, transport fluxes rely on the computation of gradients, whose accuracy depends on the numerical grid.

When conservation laws are solved on a discretized representation of the physical domain, a numerical error is inherited by the solution. This error is a function of the grid density: it approaches zero as the cell dimension approaches the infinitesimal size. While in deterministic simulations, one is interested in estimating a grid-independent solution, *i.e.* a solution for which the discretization error is almost null, in a UQ framework, it is possible to relax this constrain and to use a grid whose numerical uncertainty on a quantity of interest is significantly lower than the variability induced by the boundary condition or model parameters uncertainties. Several methodologies for estimating such a numerical error has been proposed in the literature. Historically, the first method was proposed by Richardson [13]: the numerical error, and, thus, the extrapolated solution, can be characterized using the solution of two nested meshes. This method assumes that the order of convergence of the numerical scheme

is known and respected. To get rid of this assumption, Roache [14] proposed to use three grids for closing the system. More recently, Eça [15] developed a procedure that, unlike the first two methods, can be applied even outside the asymptotic range of spatial convergence. Anyway, when hypersonic simulations are carried out such a rigorous grid converge study is replaced by the rather pragmatic one of checking that a given quantity of interest does not notably vary between two or more differently refined meshes. Few works [16, 17] addressed specifically a formal estimation of the error in this context.

On the other hand, Uncertainty Quantification (UQ) allows us to characterize the variability on quantities of interest of uncertainties in the model and boundary conditions. Such a framework must evaluate the output quantities at several (also thousands) configurations of the uncertain input variables. Even if the associated computational cost can be alleviated by replacing the Computational Fluid Dynamics (CFD) result with a surrogate model, many simulations of the flow are still needed for its training. In particular, every free stream condition requires a dedicated computational grid. It is clear that in this case, the user-based monitoring of the convergence of the solution is much more complex, and automated interventions are necessary to improve the quality of the computational grid. Otherwise, fluctuations caused by numerical errors could be misinterpreted as variations due to input uncertainties or yield difficulties in the training of the surrogate model. The uncertainty propagation through a CFD code is often performed using the same mesh optimized for the nominal conditions. This approach is usually sufficient in the absence of shock waves [18, 19], but it has also been used for hypersonic flows [20, 21]. In particular, in [22], a fixed computational grid, carefully adapted and refined for the nominal conditions, was used to perform all the simulations in the perturbed conditions required for the uncertainty study and the construction of a surrogate model. However, this approach can yield highly inaccurate results in hypersonic reacting flows over blunt bodies. When considering uncertainties on some input parameters, such as the free stream velocity or Mach number, different shock stand-off distances can be obtained. This phenomenon can cause a mesh/shock

misalignment, provoking poor heat flux trends due to a carbuncle problem. For this reason, in UQ applications, one should rely on grids that are automatically aligned to the shock.

In this study, we propose a methodology for a robust and efficient characterization of the surface pressure and heat flux of a hypersonic vehicle in a stochastic framework. We systematically employ grid adaptation tools to automatically prevent mesh-shock misalignment, guaranteeing the robustness of the prediction without manual intervention. The benefits of adopting this strategy are investigated comparing the grid-align results against those obtained on the nominal mesh. Furthermore, in contrast with the pragmatic approach commonly adopted in hypersonic simulations, we employ a rigorous grid convergence study to evaluate the numerical uncertainty expected by using a given mesh. The advantage is immediately evident in UQ studies, where we would like to resort to a very efficient numerical representation to minimize the computational effort in training the surrogate model. A grid characterized by a vanishing numerical uncertainty may be a waste of computational budget when the variability induced by the boundary conditions uncertainties still dominate the prediction. For this reason, these uncertainties are propagated to estimate the consequent variability of the quantities of interest. The latter is then compared to the numerical uncertainty to choose the most efficient mesh. We select the EXPERT vehicle [23, 24] entry flow as case study.

The work is structured as follows: firstly in Section 2, the CFD solver and the simulation details are given. In Section 3, the error for each used numerical domain is characterized, while in Section 4 some insights about the surrogate models and their construction are shown. The grid convergence of statistical moments is presented, together with comparing the output standard deviation and the numerical uncertainty. Finally, Section 5 draws some conclusions and perspectives.

2. Numerical simulations and mesh adaptation

The results of this paper rely on the US3D software, which solves chemical reacting Navier-Stokes equations in a three-dimensional finite-volume framework [25]. In this study, the numerical fluxes are computed according to the modified Steger-Warming scheme [26] with a MUSCL [27] approach to obtain second-order accuracy. The vehicle forebody flow field can be reasonably assumed to be laminar and steady. Thus, turbulence was not accounted for, neither in the modeling nor in the mesh size. The Data Parallel Line Relaxation (DPLR [28]) time integration was employed to ensure rapid convergence to steady-state. All simulations were run until a drop of around 8 orders of magnitude in the residual was achieved. The high scalability and efficiency of the solver allows to reduce the computational time for each simulation, leading UQ study to be performed very cost efficiently.

The MUTATION++ library [29], already coupled to US3D in a previous work [30], is used for the closure of: I) Transport (viscosity, thermal conductivity, diffusive fluxes), II) Gas chemistry, and III) Gas-Surface interaction. Gas finite rate chemistry relies on the Park's mechanism [31] applied to a mixture of five species air (S = [N, O, NO, N_2, O_2]).

The surface recombination reactions, promoted by the catalytic property of the reusable Thermal Protection System (TPS) material, were accounted for; specifically, $O + O \rightarrow O_2$ and $N + N \rightarrow N_2$. The surface was thus modeled imposing a surface mass-energy balance:

$$\dot{\omega}_\mathrm{i} = \mathbf{j}_\mathrm{i} \cdot \mathbf{n}, \qquad \forall \mathrm{i} \in S, \tag{1}$$

$$\sum_{\mathrm{i} \in S} \mathbf{j}_\mathrm{i} h_\mathrm{i} \cdot \mathbf{n} - \lambda \nabla T \cdot \mathbf{n} = S_\mathrm{rad}, \tag{2}$$

where $\dot{\omega}_\mathrm{i}$ is the chemical production term, $\mathbf{j}_\mathrm{i}$ the species diffusion flux, $\mathbf{n}$ the normal to the surface, h_i the species enthalpy, λ the thermal conductivity and $S_\mathrm{rad} = \sigma \epsilon T^4$ the radiative energy flux (being the surface emissivity $\epsilon = 0.9$, and the Stefan-Boltzmann constant, σ). The chemical production term was computed using a phenomenological approach, *i.e.* specifying the probability,

Table 1: Nominal conditions and associated uniform uncertainties for free stream density, ρ_∞, free stream velocity, u_∞, and recombination probability, γ

Variable	Nominal value	Distribution	Minimum	Maximum
ρ_∞ [kg/m^3]	2.88 10^{-4}	Uniform	2.30 10^{-4}	3.46 10^{-4}
u_∞ [m/s]	4868.6	Uniform	3985.8	5842.3
γ [-]	0.0015	Uniform	0.001	0.002

γ, that a given surface reaction occurs. It reads:

$$\dot{\omega}_\mathrm{i} = m_\mathrm{i}\gamma_\mathrm{i}\mathcal{N}_\mathrm{i}, \tag{3}$$

where $\mathcal{N}_\mathrm{i}$ is the number flux of species i impinging the wall and m_i its mass. A probability of one indicates that all the atoms recombines at the surface, while a probability of zero implies that no reaction occurs.

The set of equations 1 and 2 is solved by means of the gas-surface interaction module of MUTATION++ [32]. It returns to the CFD solver the partial densities at the wall and its temperature, T_w. Their extrapolated values are imposed in the ghost cells as boundary condition.

In this work, we decided to simulate the entry flow of the EXPERT vehicle, using the same nominal free stream conditions as in [22], reported in table 1. In these conditions (Mach number around 15), a strong bow shock develops in front of the vehicle, as plotted in fig. 1. The consequent increase of temperature, fig. 2, drives the molecules dissociation into atoms. These diffuse through the boundary layer and partially recombine because of the temperature drop and the catalytic activity of the surface.

The starting nominal computational grid contains 39x41 nodes; other three finer grids were obtained by progressively doubling the nodes in both the direction to obtain geometrically similar meshes. The set of four nested grids, reported in table 2, allows to assess the spacial convergence and error of the quantities of interest. The normalized characteristic length, h_i/h_1, the wall-

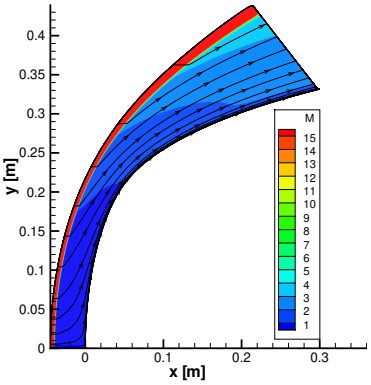

Figure 1: Mach contour at nominal condition. A strong bow shock develops in front of the vehicle.

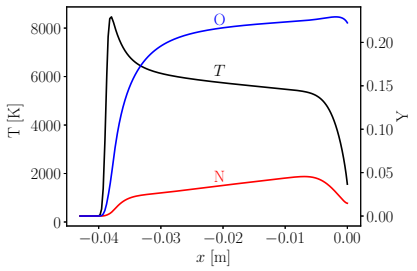

Figure 2: Temperature (left) and mass fractions (right) values along the stagnation line at nominal condition. The jump in temperature drives the molecules dissociation. The resulting atoms diffuse through the boundary layer and partially recombine because of the temperature drop and the catalytic activity of the surface.

normal distance of the first cell at the stagnation point, Δn, and the average time for 5.000 iterations to be performed on 16 cores are provided in the same table.

In the same table is also reported the value of the sonic Reynolds number in the stagnation point cell; it is defined as:

$$Re_c = \frac{\Delta n \rho a}{\mu_w}, \tag{4}$$

where ρ is the mixture density, a the wall sonic velocity, and μ_w the surface viscosity, which depend on the wall state, and, thus, on the mass-energy balance imposed as boundary condition. As a general rule of thumb, hypersonic heat fluxes are well computed using a first normal spacing of 10^{-6} m; anyway it was shown that this value is affected, for example, by the surface temperature [10]. A better criteria of convergence is the sonic Reynolds number, which should be kept lower than the unity [3, 4].

The mesh III and the mesh IV are showed, respectively, in fig. 3a and 3b: exploiting the axi-symmetry of the flow, the 3D problem is reduced to a 2D

Table 2: Numerical grids used in the study: tag of the mesh, number of nodes, number of cells, normalized characteristic length, h_i/h_1, wall-normal distance of the first cell at the stagnation point, Δn, sonic Reynolds number based on the first physical cell, and time required to perform 5.000 iterations on 16 cores.

Mesh	Nodes	Cells	h_i/h_1	Δn [m]	Re_c	Time [s]
I	305x321	97280	1	$1.25\ 10^{-6}$	0.2	≈ 2490
II	153x161	24320	2	$2.50\ 10^{-6}$	0.4	≈ 675
III	77x81	6080	4	$5.00\ 10^{-6}$	0.8	≈ 205
IV	39x41	1520	8	$1.00\ 10^{-5}$	1.6	≈ 90

configuration; further reduction of the computational cost was achieved by simulating only the half part of the 2D domain.

As mentioned in the Introduction, the generation of a good mesh is a challenging task for hypersonic simulations: it is essential to align the grid to the shock [3]. This good practice reduces the magnitude of spurious numerical error produced across the shock, that, being propagated downstream, affects the correct evaluation of surface proprieties [6]. This aspect is particularly crucial in a UQ context, where building a correct mesh for each studied condition sounds as an unaffordable effort. For this reason, we used US3D "tailoring" routine [25]: once the simulation is converged on a nominal grid, the routine computes the position of the shock and the numerical grid is aligned. The simulation is then converged on the new grid. As it can be appreciate in fig. 4, the "tailoring" tool allows to capture a much less diffuse shock, improving after-shock flow predictions. An example of "tailored" is shown on fig. 3c.

3. Numerical error and uncertainty

In this study, we followed the procedure proposed by Eça [15] to compute the numerical uncertainty. Considering the only highest order term, the numerical

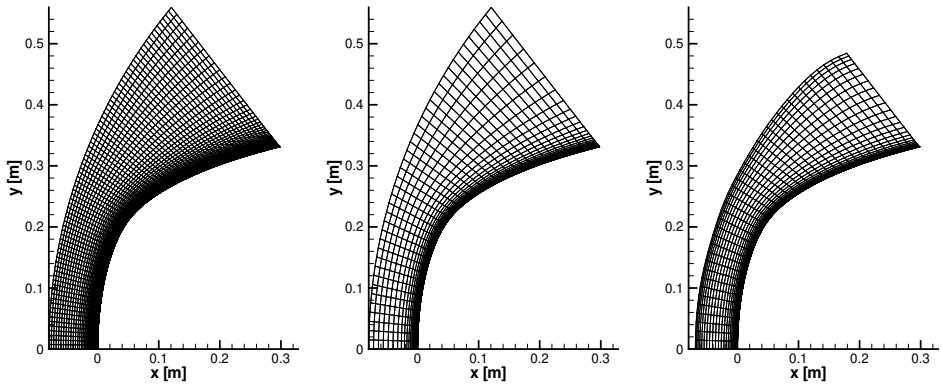

(a) Mesh III. (b) Mesh IV. (c) Mesh IV adapted.

Figure 3: Numerical grids used in the study: number of nodes halved in the both the directions and effect of mesh adaptation tool.

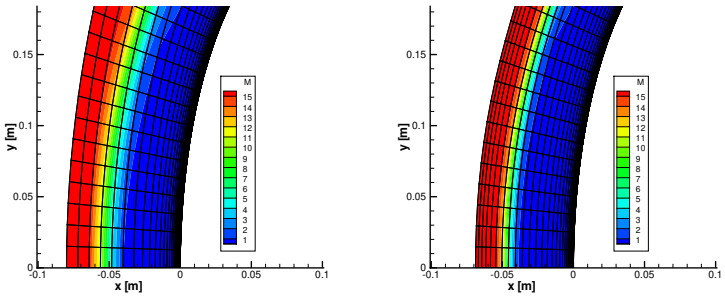

(a) Non adapted. (b) Adapted.

Figure 4: Zoom of the Mach contour on the mesh IV: the adaptation tool improves grid-shock alignment.

error, ϵ_ϕ, can be approximated as:

$$\epsilon_\phi \approx \delta_{\mathrm{RE}} = \phi_{\mathrm{i}} - \phi_0 = \alpha h_{\mathrm{i}}^p. \tag{5}$$

The quantity ϕ_{i} is a flow quantity of interest at the grid refinement i, ϕ_0, the estimate of the exact solution, α, a constant to be determined, h_{i}, the typical cell size and p is the observed order of grid convergence, that, in general, may be different from the formal one.

When the "exact" solution of the quantity of interest is not known in closed form, eq. (5) can be rearranged as follow:

$$\phi_{\mathrm{i}} = \phi_0 + \alpha h_{\mathrm{i}}^p. \tag{6}$$

The three unknowns (ϕ_0, α, and p) can be then estimated by using the solution of at least 4 meshes, and fitting the law by minimizing the standard deviation, σ. A positive value of order of convergence (p) guarantees a monotonic convergence, in contrast, a negative value indicates a monotonic divergence.

The method allows the numerical uncertainty associated to each mesh to be computed as:

$$U_\phi(\phi_{\mathrm{i}}) = \begin{cases} F_{\mathrm{s}}\epsilon_\phi(\phi_{\mathrm{i}}) + \sigma + |\phi_{\mathrm{i}} - \phi_{\mathrm{fit}}|, & \text{if } \sigma < \Delta_\phi \\ 3\frac{\sigma}{\Delta_\phi}(\epsilon_\phi(\phi_{\mathrm{i}}) + \sigma + |\phi_{\mathrm{i}} - \phi_{\mathrm{fit}}|), & \text{otherwise} \end{cases}, \tag{7}$$

where $\Delta_\phi = (\phi_{\mathrm{i}}^{\max} - \phi_{\mathrm{i}}^{\min})/(n_{\mathrm{g}} - 1)$ is a data range parameter which measures how distant the solutions are. F_{s} is a safety factor: when we have an order of convergence comparable to the theoretical one ($0.5 \leq p < 2.1$) and a good quality of the fit ($\sigma < \Delta_\phi$), we can safely rely on the error estimate and we prescribe a small safety factor, equal to 1.25. Contrary, the solutions lay outside the asymptotic range of convergence, and, thus, we prescribe a higher safety factor, equal to 3. Compared to other methods, such as the GCI method by Roache [14], this procedure takes into account also the uncertainty due to the scatter of data, and, being more conservative, is to be preferred in practical application, when there is not guaranty to always be in the asymptotic range.

The four meshes listed in table 2 were used to compute the numerical error

relative to the nominal condition reported in table 1; the results are obtained both for the adapted grids (later shown with solid lines) and for the original ones (later shown with dashed lines).

The angular distribution of pressure and heat flux are, respectively, plotted in fig. 5a and 5b. One can see that most of the numerical error concentrates around the stagnation point, where the quantities of interest reach their maximum value. Their grid dependency was investigated both as stagnation point value and as integrated value along the surface.

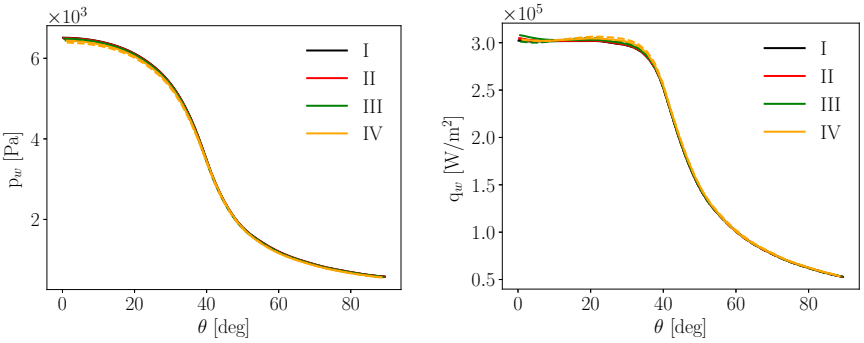

(a) Pressure.

(b) Heat flux.

Figure 5: Angular distribution of the quantities of interest for the four meshes in table 2 relative to the nominal conditions reported in table 1. Solution from adapted mesh (A) with solid line, and from non adapted mesh (NA) in dashed line. The numerical error concentrates around the stagnation point, where the quantities of interest reach their maximum value.

Equation (6) was used to compute the numerical error relative to the stagnation and integrated pressure (force), as these values fall in the monotonically convergent range. The normalized values ($100 \cdot |\frac{\phi_i - \phi_0}{\phi_0}|$) are shown respectively in fig. 6a and 6c: the numerical error decreases as the mesh is refined, with a slope proportional to the observed order of convergence, whose values are given on table 3. In this case, the grid adaptation tool improves the orders of convergence, and, thus, the rate of reduction of the numerical error. These values turn out to be lower than the theoretical value of 2, expected from the MUSCL recontraction. Two main reasons compete in the corruption of the order:

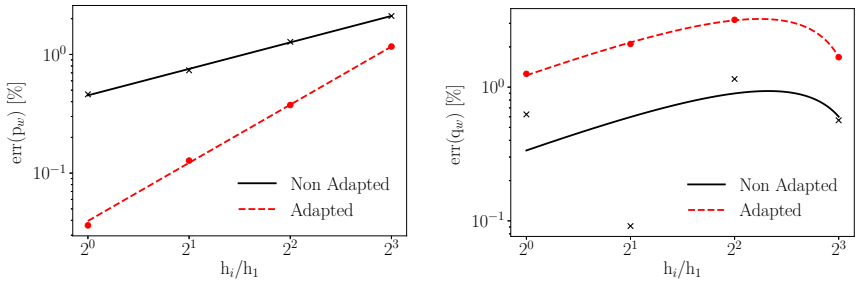

(a) Pressure.

(b) Heat flux.

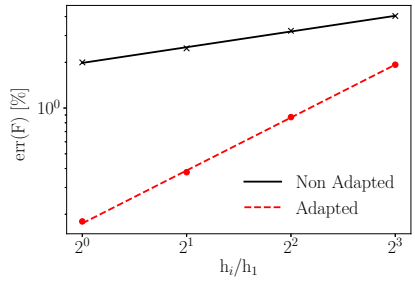

(c) Force.

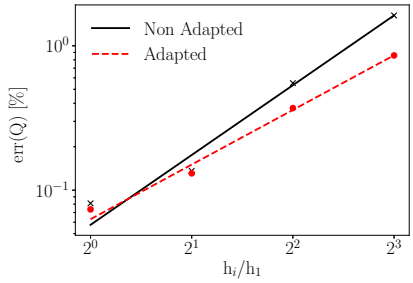

(d) Heat load.

Figure 6: Relative error on the quantities of interest as function of the degree of refinement. Pressure, force and heat load in the monotonic convergence range. The observed order of convergence increases by employing grid adaption tools for pressure and force. Heat flux outside the monotonic convergence range, adaptation improves the fit.

I) To prevent numerical oscillations from spreading, limiters are generally employed to decrease the order of the MUSCL extrapolation when a discontinuity, such as a shock, is detected. In this case, a mix of first and second-order spatial accuracy dominates the flowfield. This behaviour was already observed by Roy [17] who investigated the spatial convergence of surface pressure in a Mach 8 flow over a blunt body.

II) The gas-surface interaction module of MUTATION++ [32], used for solving the mass-energy balance boundary condition, is first-order accurate, enforcing the first-second order mix.

Unlike these properties, stagnation point heat flux exhibits a non-monotonic convergence and equation (6) cannot be applied. In such cases, Eça [15] sug-

Table 3: Orders of convergence for the quantities of interest.

	p_w [Pa]	F [N]	Q [W]
NA	0.74	0.34	1.60
A	1.63	1.15	1.25

gested to use a polynomial fit:

$$\phi_i = \phi_0 + \alpha_1 h_i + \alpha_2 h_i^2. \tag{8}$$

The use of a polynomial fit is also justified by the reasons mentioned above: the error is a mix of first and second-order errors. Similarly to the other two proprieties, the fitting is improved when the adaptation tool is used, as one can see from fig. 6b. It is interesting to note that, by contrast, the surface integrated value of the heat flux is in the monotonic convergence range, fig. 6d.
Equation (7) allows evaluating the numerical uncertainty related to the use of a given grid, as shown in fig. 7. It can be noticed that the methodology is very conservative: the uncertainty bars of a coarser mesh contains the ones of a finer one. The only exception is the heat flux uncertainty bar of the coarsest mesh, which does not contain the other three due to the use of the polynomial fit. A second significant effect of adapting the mesh can also be noticed: the uncertainty associated with each property decreases as a consequence of a better fitting and order of convergence.

4. Uncertainty assessment and construction of a surrogate model

This section is devoted to propagating the system uncertainty through the CFD solver for a chosen computational mesh. Specifically, we estimate the confidence interval of the stagnation pressure and heat flux by propagating the uncertain conditions on the free stream density, ρ_∞, velocity, u_∞, and the recombination probability, γ, of the surface of the EXPERT vehicle. For simplicity

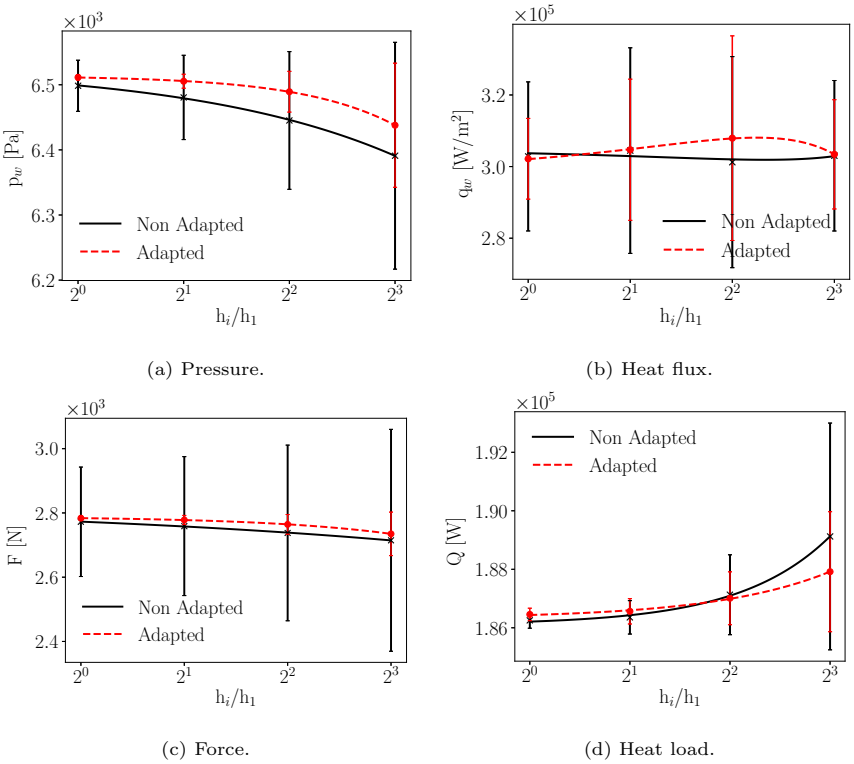

(a) Pressure.

(b) Heat flux.

(c) Force.

(d) Heat load.

Figure 7: Quantities of interest and relative numerical uncertainty as function of the degree of refinement. The methodology is conservative: the uncertainty bars of a coarser grid consistently contain the finer grid ones; the only exception is the heat flux due to the used polynomial fit. Adaptation tools systematically reduces the numerical uncertainty.

and concision, we decided to neglect the uncertainty on the atmospheric chemistry model considered in [22]. Compared to the latter work, we changed the definition of the free stream variables. Notice that this change of variables is only done for consistency with many reconstructions works in the literature. Furthermore, it does not modify the underlying problem since the free stream temperature is fixed to its nominal value and, therefore, uncertainties on the pressure are proportional to uncertainties on the density. The same can be said for Mach number and velocity since the fluid is considered a perfect gas. In this work, uninformative uniform priors are chosen for the rebuilt quantities, namely

of ±20% intervals around the nominal values for the density and the velocity, and a [0.001; 0.002] interval for γ. The complete list of uncertainties is resumed in Table 1.

In [22], Polynomial Chaos expansion was used to train surrogate models of the quantities of interest to accelerate the Markov Chain Monte Carlo (MCMC) algorithm used to sample the posterior distribution of the rebuilt quantities. However, due to the lack of the use of mesh adaptation, the numerical error associated with the results of heat flux simulations was too high, and the resulting surrogate model was not physically meaningful (negative heat flux values).

In this work, instead, for practical reasons, we prefer adopting an Ordinary Kriging surrogate model. The main reason is that it easily allows controlling the level of trust associated with the CFD training data, allowing for smoothing the numerical error related to heat flux simulations. Kriging interpolation is a well-known and widely-used technique for building a surrogate model; a detailed description of the model can be found in [33, 34, 35, 36]. We will not provide further details about this method in this work, but the reader can refer to the cited works for detailed descriptions. We used the UQLab software [37] for the construction of the surrogate model.

We generated $N_s = 80$ sampling points with the Sobol technique [38] to train the surrogate model, and $N_v = 20$ with a Latin Hypercube strategy [39] for verification purposes.

In this study, we decided to pay the price of performing a CFD simulation for each sampling point and for the mesh I,II,III, and IV in table 2 to assess the convergence behaviour of statistical moments (mean and standard deviation). The stagnation pressure and heat flux were extracted from each solution and used to train a specific surrogate model. The surrogate model allows estimating the quantities of interest in points belonging to the uncertainty space, different from the ones used for training; the representation of the models obtained for the adapted mesh II is plotted in fig. 8. It is interesting to observe the surrogate built using the mesh II when the mesh is not adapted, as in fig. 9a. For the upper limit of inlet density and velocity, an overshoot in heat flux is evident: it

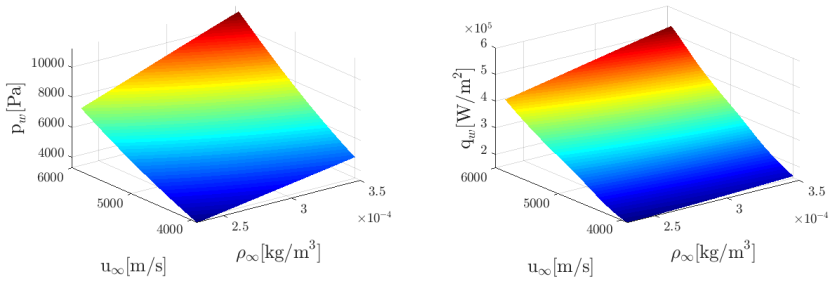

(a) Pressure.

(b) Heat flux.

Figure 8: Surrogate models obtained for the adapted mesh II using UQLab [37]: no not physical values are observed.

is a consequence of the poor alignment of the grid to the shock. In particular, in fig. 9b, we can see how grid adaptation improves the solution, leading to physically sound values.

Non-physical behavior was thus not present, as instead is reported in [22], where the surrogate was predicting negative heat flux values in the portion of the range of variation of the input. We stress out that the improved quality of the surrogate model for the heat flux, with respect to [22], is not related to the different choice of surrogate modeling technique, but it is indeed connected to the quality of the training data provided.

Furthermore, to assess the model quality, the values returned by the surrogate model were compared with those obtained by the CFD on the verification points. As the QQplots () illustrate in fig. 10, the surrogate model performs very well, as also confirmed by the verification errors, consistently below 10^{-5}. Therefore, it could be possible to safely exploit the obtained surrogates for several scopes, *e.g.* optimization, inverse problem.

Once verified the robustness of the surrogate models, they can be used to compute statistically meaningful moments, such as the mean, hereafter indicated with a $\hat{\cdot}$ of the QoI, and the standard deviation, indicated with $\sigma(\cdot)$ of the QoI, on the bounded uncertainty space of table 1, by means of a Monte Carlo method.

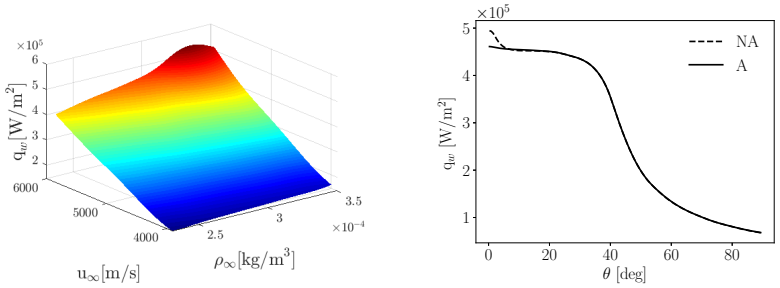

(a) Surrogate model when mesh is not adapted: not physical increase in the heat flux is predicted for high values of free stream velocity and density.

(b) Angular distribution: comparison of behaviour of adapted and non adapted mesh for a free stream velocity of 5600 m/s. A not physical increase in the stagnation point region is observed when the mesh is not adapted.

Figure 9: Heat flux obtained using mesh II.

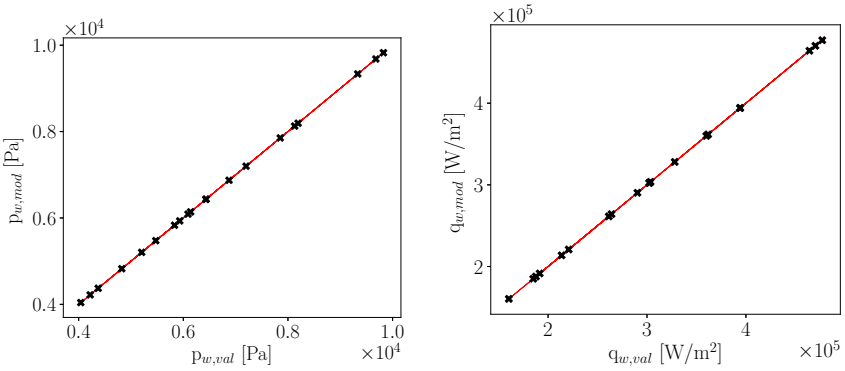

(a) Pressure.

(b) Heat flux.

Figure 10: QQplot obtained for the adapted mesh II: the surrogate model is capable to predict correct values for the verification points.

As one can see in fig. 11a, the heat flux mean value of the surrogate model has the same polynomial behaviour of the heat flux in the nominal case. The same holds for the model standard deviation plotted in fig. 11b.

At this point it makes sense to compare the standard deviation of the surrogate models and the relative numerical uncertainties. We define an average

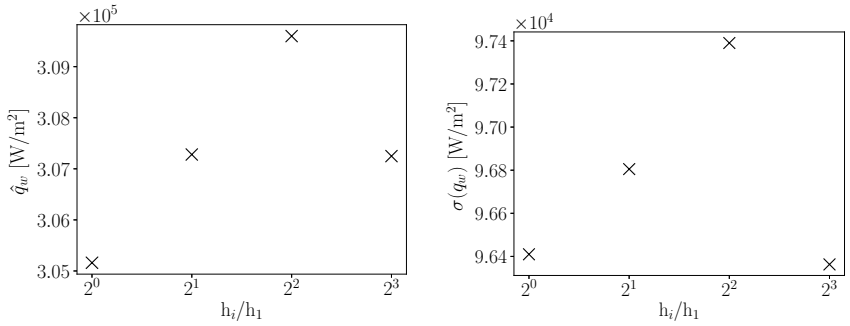

(a) Mean.

(b) Standard deviation.

Figure 11: Statistical moments of the surrogate model relative to the uncertainty space reported on table 1, as function of the degree of refinement. They follow the same polynomial behaviour observed in the nominal case.

numerical uncertainty, and a relative standard deviation, associated to each grid (g) and proprieties (ϕ) as:

$$U_g(\phi) = \frac{\sum_{s=0}^{n_s} U_{g,s}(\phi)}{n_s}, \tag{9}$$

$$S_g(\phi) = \sqrt{\frac{\sum_{s=0}^{n_s}(U_g(\phi) - U_{g,s}(\phi))^2}{n_s - 1}}, \tag{10}$$

where $U_{g,s}$ is the numerical uncertainty associated to each simulation s used to train the surrogate model for the numerical grid g. Their values, in the case of non-adapted and adapted grids, normalized concerning the surrogate model standard deviation of each grid , $(U_g(\phi) \pm S_g(\phi))/\sigma(\phi, h_i/h_1) \cdot 100$, are shown in fig. 12: small ratios indicates that the numerical uncertainty is negligible compared to the one induced by the uncertainty input.

As one can see in fig. 12a, the numerical uncertainty associated with the pressure decreases with the degree of the refinement and it is systematically lower when the mesh is adapted. Moreover, it can be seen that its magnitude is reduced more by adapting the grid than by refining it. Furthermore, in the chosen uncertainty space, even the coarsest non adapted grid has a numerical uncertainty of at least one order of magnitude lower than the standard deviation, which makes the use of mesh IV for surface pressure estimate very robust.

Regarding the heat flux, in fig. 12b, the trend is not monotonic as for the pressure, but the average numerical uncertainty, and the associated standard deviation, is systematically lower in the case of the adapted grid. Remark that the significant standard deviation for the non-adapted grid is biased by few simulations where the carbuncle effect is observed. In this case, as one can see in fig. 13, the numerical uncertainty is driven high because bad scatter of the data. Adaptation, preventing the carbuncle effect from spreading, reduces the numerical uncertainty to acceptable values and is preferred in heat flux estimates.

The mesh IV can be employed, together with grid adaption tools to guarantee robustness, to train the surrogate model in a very efficient way, as its numerical uncertainty on the prediction is at least one order of magnitude lower then the relative UQ-driven standard deviation.

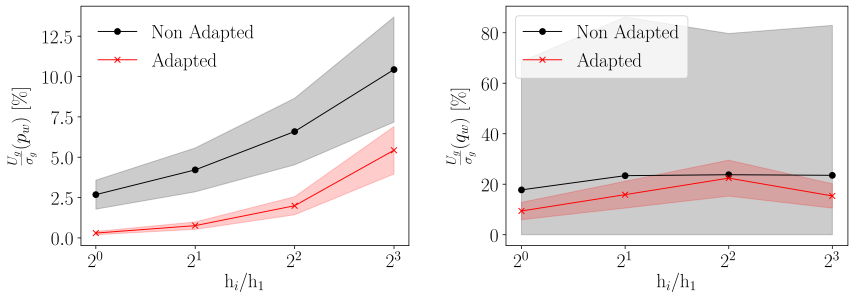

(a) Pressure.

(b) Heat Flux.

Figure 12: Ratio between the averaged grid numerical uncertainty, $U_g(\phi)$, and the standard deviation of the associated surrogate model, $\sigma(\phi, h_i/h_1)$, (solid lines) , as function of the degree of refinement. Normalized standard deviation of grid numerical uncertainty, $(S_g(\phi)/\sigma(\phi, h_i/h_1))$, with opaque area. The numerical uncertainty is systematically lower when the mesh is adapted.

5. Conclusion

In this work, we illustrated one of the first systematic quantification of the numerical error and the uncertainty-induced variability for the simulation of

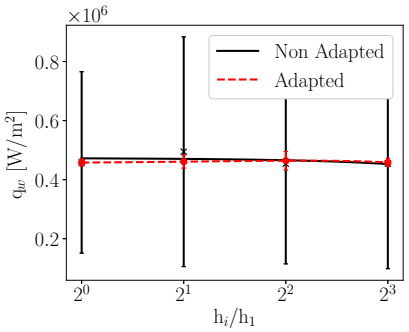

Figure 13: Numerical uncertainty as function of the degree of refinement for a free stream velocity of 5600m/s. It is driven high when carbuncle effect corrupts the solution on non adapted grids.

hypersonic flows. Specifically, we showed that the use of grid alignment tools should always be adopted. In fact, they guarantee a better trend of the numerical error and improve the order of convergence. This behavior translates into having less numerical uncertainty associated with the estimate of the quantity of interest on a given mesh. Furthermore, they are essential in UQ context, where it is not possible to manually adjust the mesh for each free stream configuration. In fact, non physical picks in the heat flux estimate were observed for some training points when the nominal mesh was used: the consequent surrogate model is not reliable. By contrast, grid adaptation tools prevent carbuncle effects to possibly corrupt the solution in specific training points: a regular behavior of the quantities of interest was observed with a resulting good quality of the associated surrogate model.

We also performed a grid convergence study to evaluate the numerical uncertainty expected by using a given mesh. It was compared to the UQ-driven standard deviation, allowing us to choose the most efficient mesh to perform the simulations required to train the surrogate model: the numerical uncertainty associated to the coarsest, and most efficient, grid turned out to be at least one order of magnitude less than the model variability for the chosen uncertainty space. An efficient and robust surrogate model can be built employing

this mesh together with mesh alignment tools.
Lastly, it was noticed that the importance of the numerical uncertainty is reduced mostly by adapting the grid rather than by refining it.
We remind that within this work, we decided to pay the price of simulating the four different meshes to build the surrogate model. From future perspectives, we suggest to explore using adaptive methodologies to balance the numerical and the problem uncertainty to minimize the computational cost.

6. Acknowledgements

Authors acknowledge the Air Force Office of Scientific Research (AFOSR) for supporting the work under the grant FA9550-18-1-0209. We also gratefully thank Professor Candler for the discussion about the accuracy of numerical schemes used in hypersonics simulations.

References

[1] C. Baranger, Y. Dauvois, G. Marois, J. Mathé, J. Mathiaud, L. Mieussens, A BGK model for high temperature rarefied gas flows, European Journal of Mechanics - B/Fluids 80 (2020) 1–12. doi:https://doi.org/10.1016/j.euromechflu.2019.11.006.

[2] Z. Bouyahiaoui, R. Haoui, A. Zidane, Numerical investigation of a hypersonic flow around a capsule in CO2–N2 environment, European Journal of Mechanics - B/Fluids 80 (2020) 146–156. doi:https://doi.org/10.1016/j.euromechflu.2019.12.009.

[3] P. Papadopoulos, E. Venkatapathy, D. Prabhu, M. P. Loomis, D. Olynick, Current grid-generation strategies and future requirements in hypersonic vehicle design, analysis and testing, Applied Mathematical Modelling 23 (9) (1999) 705–735. doi:10.1016/S0307-904X(99)00007-4.

[4] G. Candler, M. Barnhardt, T. Drayna, I. Nompelis, D. Peterson, P. Subbareddy, Unstructured Grid Approaches for Accurate Aeroheating Simulations, in: 18th AIAA Computational Fluid Dynamics Conference, American Institute of Aeronautics and Astronautics, 2007. doi:10.2514/6.2007-3959.

[5] S. Henderson, J. Menart, Grid Study on Blunt Bodies with the Carbuncle Phenomenon, in: 39th AIAA Thermophysics Conference, American Institute of Aeronautics and Astronautics, 2007. doi:10.2514/6.2007-3904.

[6] G. Candler, D. Mavriplis, L. Trevino, Current status and future prospects for the numerical simulation of hypersonic flows, in: 47th AIAA Aerospace Sciences Meeting including The New Horizons Forum and Aerospace Exposition, American Institute of Aeronautics and Astronautics, 2009. doi:10.2514/6.2009-153.

[7] A. Bonfiglioli, M. Grottadaurea, R. Paciorri, F. Sabetta, An unstructured, three-dimensional, shock-fitting solver for hypersonic flows, Computers & Fluids 73 (Supplement C) (2013) 162 – 174.

[8] M. Onofri, R. Paciorri, D. Cardillo, M. Grottadaurea, A. Bonfiglioli, Numerical Simulations of flows past IXV re-entry vehicle at CRAS, in: 3rd International ARA days, 2011.

[9] Z.-X. Gao, H.-C. Xue, Z.-C. Zhang, H.-P. Liu, C.-H. Lee, A hybrid numerical scheme for aeroheating computation of hypersonic reentry vehicles, International Journal of Heat and Mass Transfer 116 (2018) 432–444. doi:10.1016/j.ijheatmasstransfer.2017.07.100.

[10] S.-C. Luo, J. Liu, K. Li, Grid convergence and influence of wall temperature in the calculation of thermochemical non-equilibrium heat flux, Journal of Physics D: Applied Physics 53 (28) (2020) 285502. doi:10.1088/1361-6463/ab813c.

[11] D. Saunders, S. Yoon, M. Wright, An Approach to Shock Envelope Grid Tailoring and Its Effect on Reentry Vehicle Solutions, in: 45th AIAA Aerospace Sciences Meeting and Exhibit, American Institute of Aeronautics and Astronautics, 2007. doi:10.2514/6.2007-207.

[12] J. M. Longo, Aerothermodynamics – A critical review at DLR, Aerospace Science and Technology 7 (6) (2003) 429–438. doi:10.1016/S1270-9638(03)00036-1.

[13] L. F. Richardson, R. T. Glazebrook, IX. The approximate arithmetical solution by finite differences of physical problems involving differential equations, with an application to the stresses in a masonry dam, Philosophical Transactions of the Royal Society of London. Series A, Containing Papers of a Mathematical or Physical Character 210 (459) (1911) 307–357. doi:10.1098/rsta.1911.0009.

[14] P. J. Roache, Perspective: A Method for Uniform Reporting of Grid Refinement Studies, Journal of Fluids Engineering 116 (3) (1994) 405–413. doi:10.1115/1.2910291.

[15] L. Eça, M. Hoekstra, A procedure for the estimation of the numerical uncertainty of CFD calculations based on grid refinement studies, Journal of Computational Physics 262 (2014) 104–130. doi:10.1016/j.jcp.2014.01.006.

[16] F. G. Blottner, Accurate Navier-Stokes results for the hypersonic flow over a spherical nosetip, Journal of Spacecraft and Rockets 27 (2) (1990) 113–122. doi:10.2514/3.26115.

[17] C. J. Roy, Grid Convergence Error Analysis for Mixed-Order Numerical Schemes, AIAA Journal 41 (4) (2003) 595–604. doi:10.2514/2.2013.

[18] S. Kawai, K. Shimoyama, Kriging-model-based uncertainty quantification in computational fluid dynamics, in: 32nd AIAA Applied Aerodynamics Conference, American Institute of Aeronautics and Astronautics, 2014. doi:10.2514/6.2014-2737.

[19] S. Salehi, M. Raisee, M. J. Cervantes, A. Nourbakhsh, Efficient uncertainty quantification of stochastic CFD problems using sparse polynomial chaos and compressed sensing, Computers & Fluids 154 (2017) 296–321. doi:10.1016/j.compfluid.2017.06.016.

[20] S. Hosder, R. Walters, R. Perez, A Non-Intrusive Polynomial Chaos Method For Uncertainty Propagation in CFD Simulations, in: 44th AIAA Aerospace Sciences Meeting and Exhibit, American Institute of Aeronautics and Astronautics, 2006. doi:10.2514/6.2006-891.

[21] P. Constantine, M. Emory, J. Larsson, G. Iaccarino, Exploiting active subspaces to quantify uncertainty in the numerical simulation of the HyShot II scramjet, Journal of Computational Physics 302 (2015) 1–20. doi:10.1016/j.jcp.2015.09.001.

[22] J. Tryoen, P. M. Congedo, R. Abgrall, N. Villedieu, T. Magin, Bayesian-based method with metamodels for rebuilding freestream conditions in atmospheric entry flows, AIAA Journal **52** (10) (2014) 2190 – 2197.

[23] L. Walpot, H. Ottens, J.-M. Muylaert, O. Bayle, P. Urmston, U. Thomas, G. Saccoccia, M. Caporicci, C. Stavrinidis, Heat Flux and Static Stability Predictions of the Expert Vehicle, in: D. Danesy (Ed.), Fifth European Symposium on Aerothermodynamics for Space Vehicles, Vol. 563 of ESA Special Publication, 2005, p. 139.

[24] A. Barrio, M. Sudars, J. Gavira, R. Aulisio, F. Ratti, F. Massobrio, L. Walpot, G. Passarelli, J. Thoemel, A. Thirkettle, EXPERT - The ESA experimental re-entry test-bed. Trajectory and mission design, 2011. doi:10.2514/6.2011-6342.

[25] G. V. Candler, H. B. Johnson, I. Nompelis, V. M. Gidzak, P. K. Subbareddy, M. Barnhardt, Development of the US3D Code for Advanced Compressible and Reacting Flow Simulations, in: 53rd AIAA Aerospace Sciences Meeting, American Institute of Aeronautics and Astronautics, 2015. doi:10.2514/6.2015-1893.

[26] J. L. Steger, R. Warming, Flux vector splitting of the inviscid gasdynamic equations with application to finite-difference methods, Journal of Computational Physics 40 (2) (1981) 263–293. doi:10.1016/0021-9991(81)90210-2.

[27] B. van Leer, Towards the ultimate conservative difference scheme. V. A second-order sequel to Godunov's method, Journal of Computational Physics 32 (1) (1979) 101–136. doi:10.1016/0021-9991(79)90145-1.

[28] M. J. Wright, G. V. Candler, D. Bose, Data-Parallel Line Relaxation Method for the Navier-Stokes Equations, AIAA Journal 36 (9) (1998) 1603–1609. doi:10.2514/2.586.

[29] J. B. Scoggins, V. Leroy, G. Bellas-Chatzigeorgis, B. Dias, T. E. Magin, Mutation + + : MUlticomponent Thermodynamic And Transport properties for IONized gases in C++, SoftwareX 12 (2020) 100575. doi:10.1016/j.softx.2020.100575.

[30] M. Capriati, K. Prata, T. Schwartzentruber, G. Candler, T. Magin, Development of a nitridation gas-surface boundary condition for high-fidelity hypersonic simulations, in: 14th WCCM-ECCOMAS Congress, CIMNE, 2021. doi:10.23967/wccm-eccomas.2020.119.

[31] C. Park, R. L. Jaffe, H. Partridge, Chemical-Kinetic Parameters of Hyperbolic Earth Entry, Journal of Thermophysics and Heat Transfer 15 (1) (2001) 76–90. doi:10.2514/2.6582.

[32] G. Bellas Chatzigeorgis, A. Turchi, A. Viladegut, O. Chazot, P. F. Barbante, T. Magin, Development of catalytic and ablative gas-surface interaction models for the simulation of reacting gas mixtures, in: 23rd AIAA Computational Fluid Dynamics Conference, American Institute of Aeronautics and Astronautics, 2017. doi:10.2514/6.2017-4499.

[33] G. Matheron, The theory of regionalised variables and its applications , Ph.D. thesis, École Nationale Supérieure des Mines (1971).

[34] N. A. C. Cressie, Statistics for spatial data, John Wiley & Sons, 1993.

[35] S. N. Lophaven, H. B. Nielsen, J. Søndergaard, DACE: a MATLAB Kriging toolbox, version 2.0 , Tech. rep., Technical University of Denmark (2002).

[36] C. E. Rasmussen, C. K. I. Williams, Gaussian processes for machine learning, The MIT Press, 2006.

[37] S. Marelli, B. Sudret, UQLab: A Framework for Uncertainty Quantification in Matlab, in: Vulnerability, Uncertainty, and Risk, American Society of Civil Engineers, 2014, pp. 2554–2563. doi:10.1061/9780784413609.257.

[38] I. Sobol', On the distribution of points in a cube and the approximate evaluation of integrals, USSR Computational Mathematics and Mathematical Physics 7 (4) (1967) 86–112. doi:https://doi.org/10.1016/0041-5553(67)90144-9.

[39] M. D. McKay, R. J. Beckman, W. J. Conover, A Comparison of Three Methods for Selecting Values of Input Variables in the Analysis of Output from a Computer Code, Technometrics 21 (2) (1979) 239–245. doi:10.2307/1268522.